

A comparative assessment of the distribution of Joule heating in altitude as estimated in TIE-GCM and EISCAT over one solar cycle

D. Baloukidis¹, T. Sarris¹, S. Tourgaidis¹, P. Pirnaris¹, A. Aikio², I. Virtanen²,
S. Buchert³, K. Papadakis⁴

¹Department of Electrical and Computer Engineering, Democritus University of Thrace, Xanthi, Greece

²Space Physics and Astronomy Research Unit, University of Oulu, Finland

³Swedish Institute of Space Physics (IRF), Uppsala, Sweden

⁴Formerly at the Democritus University of Thrace; now at the University of Helsinki, Helsinki, Finland

Key Points:

- Joule heating and Pedersen conductivity are calculated in TIE-GCM and EISCAT during solar cycle 24, as a function of Kp, MLT and altitude.
- Joule heating and Pedersen conductivity in TIE-GCM are under-estimated for high Kp compared to EISCAT measurements.
- Comparisons point towards the need for a Kp-dependent parameterization of small scale effects in TIE-GCM.

Corresponding author: T. Sarris, tsarris@ee.duth.gr

Abstract

During geomagnetically active times, Joule heating in the Lower Thermosphere - Ionosphere is a significant energy source, greatly affecting density, temperature, composition and circulation. At the same time, Joule heating and the associated Pedersen conductivity are amongst the least known parameters in the upper atmosphere in terms of their quantification and spatial distribution, and their parameterization by geomagnetic parameters shows large discrepancies between estimation methodologies, primarily due to a lack of comprehensive measurements in the region where they maximize. In this work we perform a long-term statistical comparison of Joule heating as calculated by the NCAR Thermosphere - Ionosphere - Electrodynamics General Circulation Model (TIE-GCM) and as obtained through radar measurements by the European Incoherent Scatter Scientific Association (EISCAT). Statistical estimates of Joule heating and Pedersen conductivity are obtained from a simulation run over the 11 year period spanning from 2009 until 2019 and from radar measurements over the same period, during times of radar measurements. The results are statistically compared in different Magnetic Local Time sectors and Kp level ranges in terms of median values and percentiles of altitude profiles. It is found that Joule heating and Pedersen conductivity are higher on average in TIE-GCM than in EISCAT for low Kp and are lower than EISCAT for high Kp. It is also found that neutral winds cannot account for the discrepancies between TIE-GCM and EISCAT. Comparisons point towards the need for a Kp-dependent parameterization of Joule heating in TIE-GCM to account for the contribution of small scale effects.

1 Introduction

During geomagnetically active times, the appearance of strong electric currents in the high-latitude ionospheric E region leads to the acceleration of ions. Part of the energy carried by the accelerated ions is dissipated through collisions with the neutrals, resulting in ion-neutral frictional heating, which is analogous to Joule heating or Ohmic heating in resistive electrical circuits. In the Lower Thermosphere-Ionosphere (LTI), Joule heating involves the collisional interactions between ionized and neutral gases in the presence of differential velocities between them in the presence of electric and magnetic fields. The collisions between ions and neutrals result in frictional momentum exchange and heating. During active times, Joule heating is known to maximize in the 100 to 200 km range in the LTI, and it is believed to exceed the long-term-average largest energy source for the system, the solar EUV radiation (e.g., Cole (1962); Lu et al. (2016); Thayer (2000); Knipp et al. (2005)).

Even though the physics of the process by which electromagnetic energy is converted into heat into the LTI is well understood (e.g., Lu et al. (1995a); Brekke and Kamide (1996); Thayer and Semeter (2004); X. Zhu et al. (2005); Vasyliūnas and Song (2005); Strangeway (2012); Aikio et al. (2012)), and is captured in physics-based Global Circulation Models (GCMs), the quantification and spatial distribution of Joule heating is still largely unknown (e.g., Palmroth et al. (2005); Palmroth et al. (2020); T. Sarris et al. (2023)). A key reason is that Joule heating in the LTI is influenced simultaneously by neutral winds, plasma turbulence, variable electric fields, and modifications in conductivity by precipitating particles and by strong electric fields, all of which are largely variable during active times. In addition, the effects of small scale structures in the electric field, that are known to be present within the auroral oval, are not well quantified. It thus comes as no surprise that large discrepancies appear in estimates of Joule heating between different models, which often disagree by large factors (Perlongo et al. (2018), T. E. Sarris (2019)), making their cross-comparison and evaluation difficult (Scherliess et al. (2019)). Furthermore, large discrepancies appear between proxies of Joule heating that are based on solar and geomagnetic activity indices.

A key unknown in the spatial distribution of Joule heating is the altitude where it maximizes and the dependence of this altitude on geomagnetic activity. For example, Griffis et al. (1981) used a few days of data (late December of 1974) from the Atmosphere Explorer C satellite as input to a computer program and derived the maximum Joule Heating value at 115km. Deng and Ridley (2007) evaluated the GITM model in a case study and found the maximum at 120km. Huang et al. (2012) run TIE-GCM model for about a month and found the largest Joule heating deposition at 125km. Banks (1977) used data from the Chatanika, Alaska auroral-zone incoherent-scatter radar to compute altitude profiles for the polar cleft region for the August 4, 1972, solar proton event, and found the maximum Joule heating rate at 128km. The dependence of Joule heating in MLT has been noted by Brekke and Rino (1978), whereas the dependence on neutral winds and geomagnetic activity on the altitude profiles of Joule heating has been highlighted by Thayer (1998) and Cai et al. (2013).

The exact quantification of Joule heating requires the simultaneous and co-located measurement of an extensive list of parameters, which is only available in situ. However, the in-situ observation of the Lower Thermosphere - Ionosphere at the 100-200 km transition region where Joule heating maximizes presents many challenges, as this altitude range is too high for balloons and too low for systematic measurements by orbiting satellites. Sounding rockets are able to sample this region (e.g., Sangalli et al. (2009)), however their measurements are near-instantaneous, providing, essentially, snapshots of altitude profiles above the location of the launch site. It is for this reason that systematic measurements of global coverage do not exist, impeding the accurate representation of Joule heating in models of the upper atmosphere (Ruan et al. (2018)).

Most of the previous studies have focused on quantifying Joule heating during single events or for periods of a few days. Instead, in this study we investigate the distribution of Joule heating statistically over long (multi-year) periods of time in terms of altitude, magnetic local time and geomagnetic activity, as estimated (a) via the NCAR Thermosphere Ionosphere Electrodynamics General Circulation Model (TIE-GCM) and (b) via measurements from the European Incoherent Scatter (EISCAT) Tromsø UHF radar. Together with Joule heating, Pedersen conductivity is also evaluated. Both TIE-GCM model outputs and EISCAT statistics are gathered for the 11-year period from 2009 to 2019, corresponding approximately to solar cycle number 24. Statistics are inter-compared in terms of percentiles within altitude bins, local time sectors and geomagnetic activity levels. It is noted that the EISCAT Tromsø UHF radar does not operate continuously, but during campaigns, as discussed in further detail below.

In the following, in chapter 2 we present the methodology that is used in the estimation of Joule heating and Pedersen conductivity in TIE-GCM, including the parameterization of the TIE-GCM run, and the methodology by which Joule heating and Pedersen conductivity are obtained via EISCAT measurements. In chapter 3 we discuss the statistical sampling and the segmentation of data that was performed in terms of altitude, magnetic local time and geomagnetic activity, and we present the results of the statistical analysis. In chapter 4 we discuss the results and potential reasons for the observed discrepancies, and in chapter 5 we summarize the key findings of this study, concluding with implications from the observed discrepancies and potential methodologies and measurements that are needed to resolve them.

2 Methodology

2.1 TIE-GCM

The NCAR Thermosphere Ionosphere Electrodynamics General Circulation Model (TIE-GCM) is a first-principles model of the coupled thermosphere and ionosphere system that solves the three-dimensional momentum, energy and continuity equations for neutral and ion species at each time step (e.g., Qian et al. (2014)). Solutions are performed on 29 constant-pressure levels, extending from approximately 97 km to 500 km in intervals of one-half scale height. Main assumptions of TIE-GCM include hydrostatic equilibrium, incompressibility on constant pressure surfaces, constant gravity, and steady-state ion and electron energy equations.

The electric field in TIE-GCM is imposed based on an externally driven geopotential field, which, in the case of the model runs of this study, is introduced based on the Weimer electric potential specification (Weimer (2005)). Furthermore, TIE-GCM assumes that the electric field is always perpendicular to the magnetic field of the Earth. An IGRF model is used for the Earth's magnetic field (Thébault et al. (2015)). The high latitude energy input associated with auroral particle precipitation is represented by an analytical auroral model (Emery et al. (2012); Roble and Ridley (1987)).

Further to the above, additional external drivers and parameterizations that are used in the TIE-GCM include: an empirical model that is used to specify photoelectron heating; an empirical model that is derived from two-stream calculations to specify the production of secondary electrons; empirical formulations that are used to specify the upper boundary conditions for electron heat transfer and electron number flux; an eddy diffusion formulation to include the effects of mixing caused by gravity waves; and the Global Scale Wave Model (GSWM) to specify atmospheric tides at the lower boundary.

The Joule heating rate in TIE-GCM is calculated based on the following equation (e.g., Lu et al. (1995b), eq. 3):

$$q_j = \sigma_P \left(\vec{E} + \vec{u}_n \times \vec{B} \right)^2 \quad (1)$$

where \vec{u}_n is the neutral wind vector, σ_P is the Pedersen conductivity, \vec{B} is the local geomagnetic field vector and \vec{E} is the electric field component that is perpendicular to the geomagnetic field. In TIE-GCM it is assumed that magnetic field lines are equipotentials, and thus that $\vec{E}_{\parallel} = 0$ and therefor $\vec{E} = \vec{E}_{\perp}$.

Pedersen conductivity in TIE-GCM is calculated by the following equation (e.g., Schunk and Nagy (2009), eq. 5.117):

$$\sigma_P = \frac{q_e}{B} \left[N_{O^+} \frac{r_{O^+}}{1 + r_{O^+}^2} + N_{O_2^+} \frac{r_{O_2^+}}{1 + r_{O_2^+}^2} + N_{NO^+} \frac{r_{NO^+}}{1 + r_{NO^+}^2} + N_e \frac{r_e}{1 + r_e^2} \right] \quad (2)$$

where r_{O^+} , $r_{O_2^+}$, r_{NO^+} and r_e are the collision frequency to gyrofrequency ratios of O^+ , O_2^+ , NO^+ and e respectively, as obtained using the collision frequencies of Schunk and Nagy (2000), and N_{O^+} , $N_{O_2^+}$, N_{NO^+} and N_e are the number densities of these species, in units of m^{-3} . It is noted that collision frequencies of the above species are calculated for collisions with the following neutral species: O , O_2 , N_2 .

TIE-GCM can be executed with various time steps and grid resolutions. For the current study a grid size of 2.5 degrees in geographic latitude and 2.5 degrees in geographic longitude was used. In the vertical dimension, TIE-GCM uses log pressure $Z = \ln(p_0/p)$ as the vertical coordinate with the reference pressure set to $p_0 = 5 \times 10^7$ hPa. Four grid points per scale height were used, leading to 57 pressure levels. For each pressure level the corresponding altitude was also calculated. For the purpose of this study,

TIE-GCM was run over the period from 2009 until 2019, with a run-time resolution of 30 sec and an output time resolution of 2 hours. In total, Joule heating was estimated at $\sim 10^8$ points.

2.2 EISCAT radar measurements and data analysis

Incoherent Scatter Radars (ISRs) have often been used to provide detailed information on both the vertical structure and the temporal evolution of the LTI, including estimates of Joule heating (e.g., Wickwar (1974); Banks (1977); Vickrey et al. (1982); Thayer (1998); Thayer (2000); Fujii et al. (1999); Aikio and Selkälä (2009); Aikio et al. (2012); Cai et al. (2013)). In the present study, Joule heating was estimated statistically from measurements provided by the European Incoherent Scatter (EISCAT) radar facility in Ramfjordmoen, near Tromsø, Norway (geographic: $69.59^\circ N$, $19.22^\circ E$, cgm: 66.58° , 102.94°). The site hosts a UHF radar, which operates in the 930 MHz band with transmitter peak power 2.0 MW, a 12.5% duty cycle and 1 μ s – 10 ms pulse length with frequency and phase modulation capability. The antenna is a 32 meter mechanically fully steerable parabolic dish used for transmission and reception. EISCAT measurements used in this study were collected from an ensemble of campaigns conducted in the period from 2009 to 2019. EISCAT measurements correspond to a total of 29,806 Pedersen conductivity and 23,938 Joule heating samples that are used in this study. It is noted that the radar did not operate continuously, and thus the total number of data points from all the campaigns are not evenly distributed during the above-mentioned 11 year period; however statistically significant measurements were obtained for all Kp, MLT and altitude ranges used in the binning of the data.

For the electric field estimation from the EISCAT Tromsø UHF radar the beam-swing method was utilized, where the antenna points in different directions in a short cycle to capture three non-coplanar ion velocity components; these experiments are referred to as cp2 or ip2. The electric field analysis was carried out as follows: F-region line-of-sight ion velocity measurements from at least three different beam pointing directions were combined and the full ion velocity vector was solved by statistical inversion as described by Nygrén et al. (2011). The electric field was obtained by assuming that ions follow the $\vec{E} \times \vec{B}$ drift in the F region and the magnetic field vector was obtained from the IGRF model.

The radar scan cycle duration is typically 4 or 6 minutes, and 6 minute resolution was used for the electric field analysis for consistency. As a result, one or two field-aligned beams that produce Pedersen conductivity profiles are included in each 6-min period. Electric field values were calculated for all Pedersen conductivity profiles by means of linear interpolation. As the electric field analysis sometimes fails even if the field-aligned electron density profile was successfully measured, and the electric field over failed fits is not interpolated, the number of Pedersen conductivity profiles in the final data set is somewhat larger than the number of Joule heating profiles.

Altitude profiles of Pedersen conductivity were calculated via the electron density profiles measured by the EISCAT UHF radar looking in the field-aligned direction, using the methodology described in, e.g., Brekke and Hall (1988); Moen et al. (1990); and Aikio et al. (2012). The ion-neutral and electron-neutral collision frequencies needed in the Pedersen conductivity were calculated according to Brekke and Hall (1988), and the required neutral parameters were obtained from the NRLMSISE-00 empirical model (Picone et al. (2002)). The Joule heating rate was subsequently calculated according to:

$$q_j = \sigma_P \vec{E}^2 \quad (3)$$

where σ_P is the Pedersen conductivity and \vec{E} is the electric field. It is noted that the electric field in EISCAT is measured in a coordinate system that is fixed to the Earth.

2.3 Statistical distributions

For the purpose of this study, and in order to compare TIE-GCM and EISCAT data, TIE-GCM outputs were used from the geographic latitudes that are closest to the geographic latitude of the EISCAT Tromsø radar, which is located at 69.6° . These include the TIE-GCM grid points with geographic latitudes 68.75° and 71.25° . In altitude, TIE-GCM outputs were averaged in ranges of 4 km each, spanning altitudes from 100 km to 150 km. In Magnetic Local Time (MLT), outputs were averaged in four MLT sectors, ranging from 15:00 to 21:00, 21:00 to 03:00, 03:00 to 09:00 and 09:00 to 15:00. In terms of geomagnetic activity, outputs were binned in three ranges in terms of the Kp index, with ranges of $0 \leq Kp < 2$, $2 \leq Kp < 4$, $4 \leq Kp < 9$, which in the following are referred to as low, medium and high activity, respectively. Within each of the above bins, the 10th, 25th, 50th, 75th and 90th percentile values were calculated. EISCAT outputs were also binned similarly in terms of Magnetic Local Time and geomagnetic activity. Within each of the above bins, similarly to the calculations of TIE-GCM gridded data, the 10th, 25th, 50th, 75th and 90th percentile values were calculated. As it is expected, the 11 year period is dominated by quiet days, with the ratio of low to medium activity periods being 2.2 to 1 and the ratio of low to high activity periods being 5.6 to 1.

3 Results

The statistical distribution of Joule heating as a function of altitude, MLT and Kp as obtained in TIE-GCM and EISCAT are shown in the top and bottom panels of Figure 1 respectively. The results of TIE-GCM are colored in blue hues and of EISCAT in green hues, and the same coloring scheme is followed throughout this paper to differentiate between TIE-GCM and EISCAT measurements. The three rows in each panel correspond to the three ranges in Kp: low (0-2), medium (2-4) and high (4-9) levels of geomagnetic activity. The four columns in each figure correspond to the four MLT sectors, divided in the afternoon (15-21), midnight (21-03), morning (03-09) and noon (09-15) regions. Colour shades under the altitude distribution curves in these figures indicate the percentiles of Joule Heating, with the darker shaded area under the thicker black line corresponding to the median values of Joule heating as a function of altitude. Lighter-shaded areas under the thin gray curves show progressively higher and lower percentiles to the right and left of the median, respectively.

For TIE-GCM statistics, the number marked in blue at the lower right corner of each panel indicates the height-integrated value of the median of Joule heating, in units of mW/m^2 . The number in black at the top right corner indicates the total number of grid points that were used in the statistical calculations. Similarly, for EISCAT statistics, the number in green indicates the height-integrated value of the median of Joule heating, whereas the number in black indicates the total number of radar profiles that were used in the statistical calculations.

The comparison between the upper and lower panels of Figure 1 shows that Joule heating estimates are lower in TIE-GCM than in EISCAT for higher levels of geomagnetic activity, and, inversely, that they are generally higher in TIE-GCM than in EISCAT for lower levels of geomagnetic activity. An exception is observed for the noon sector (MLT 09-15), where EISCAT measurements show very low levels of Joule heating for all levels of geomagnetic activity. It is also observed that EISCAT observations show considerably larger deviations from the median, in particular for higher Joule Heating values.

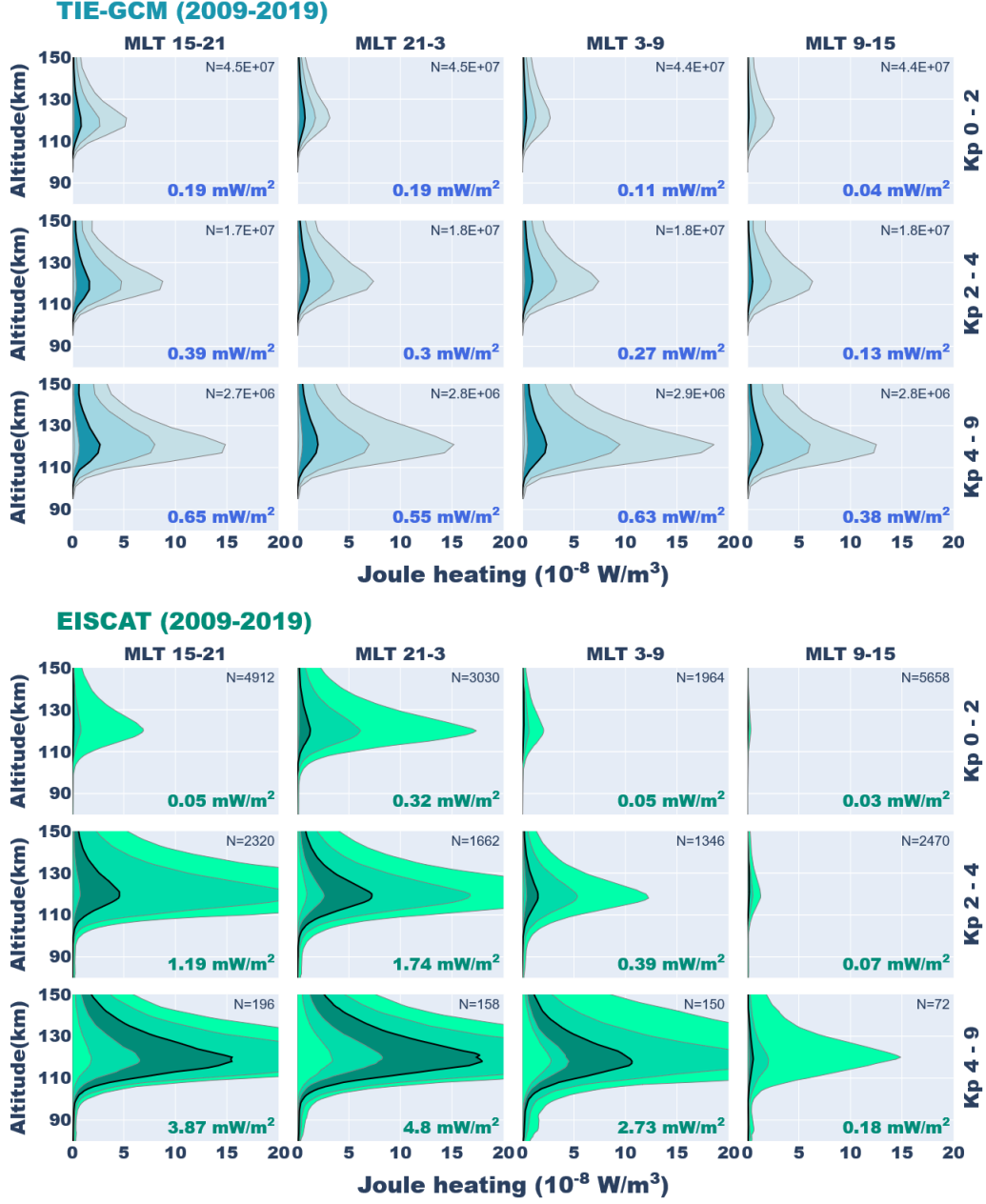


Figure 1. Altitude profiles of Joule Heating in TIE-GCM (top panel) and EISCAT (bottom panel), in units of 10^{-8} W/m^3 . Marked in blue (green) bold numbers are the height integrated values of the median of Joule Heating in TIE-GCM (EISCAT), in units of mW/m^2 ; marked in smaller black characters are the number N of grid points (top) and samples (bottom) that were used to produce the altitude profiles.

With respect to the altitude of the peak of Joule heating, in TIEGCM the maximum is found within the 119-123 km altitude bin, whereas in EISCAT it is found within the 120-121 km altitude range for low kp, 119-121 km for medium Kp and 118-121 km for high kp levels. Thus, on average, the altitude of the peak of Joule heating is found to decrease slightly on average for higher levels of geomagnetic activity. It is also noted, however, that the distribution shows a large deviation from the median, due to the smaller number of profiles for high kp, and thus this dependence of the peak altitude on geomagnetic activity could be a statistical artifact.

Figure 2 displays the Pedersen Conductivity as a function of altitude, MLT and Kp, as calculated from TIE-GCM (top panel) and EISCAT radar measurements (bottom panel), in a similar format as that of Figure 1.

From Figure 2 it can be seen that, similarly to Joule heating estimates, Pedersen Conductivity is again overestimated in TIE-GCM for low Kp, whereas it is underestimated for high Kp. Furthermore, also similarly to Figure 1, values from TIE-GCM display a more uniform distribution than those from EISCAT. Finally, the peak of Pedersen conductivity is found in the altitude range from 119-123 for TIE-GCM and within the 120-121 km altitude range for low kp, 119-121 km for medium Kp and 118-120 km for high kp levels for EISCAT, demonstrating a dependence on geomagnetic activity, with higher Kp leading to lower altitudes of the peak of Pedersen conductivity.

4 Discussion

In comparing the long-term (solar cycle) averages of Joule heating and Pedersen conductivity between TIE-GCM and EISCAT, it can be seen in Figures 1 and 2 that, in general, TIE-GCM tends to under-estimate (over-estimate) Joule heating and Pedersen conductivity for high (low) levels of geomagnetic activity compared to EISCAT measurements, with the exception of the noon sector (09-15), where EISCAT measurements are generally low. This could be attributed to the fact that, in the dayside, the auroral oval and the plasma convection cells are typically pole-ward of Tromsø, and therefore the electric field as well as auroral conductances (and hence Joule heating) are small.

A key aspect to note when assessing the causes of the observed discrepancies between EISCAT and TIE-GCM is that EISCAT calculations of Joule heating do not take into account the effects of neutral winds, as the latter cannot be measured directly from ISRs. Thus Joule heating in EISCAT is calculated through equation (3) by using only measurements of the electric field, which are performed in a coordinate system that is fixed to the earth, whereas Joule heating in TIE-GCM is calculated through equation (1), which is in the reference frame of the neutrals. It is noted that, within the LTI E-region, neutral winds can act either as a sink or a source of energy, and are known to have a significant effect in the transfer of electromagnetic energy and in the total Joule heating in the region (see, e.g., Thayer (1998)). The neutral wind is considered to be a sink of the total energy when a part of the total electromagnetic energy entering the ionosphere ends up as mechanical energy of the neutral wind, the rest being in the form of Joule heating. In particular, when neutral winds are driven frictionally by $\vec{E} \times \vec{B}$ convection, e.g., during substorm growth and expansion phases, the presence of neutral winds has the tendency to lower Joule heating, and thus an estimation without taking into account the presence of neutral winds will lead to an over-estimation of Joule heating. Inversely, when neutral winds act as a dynamo, as is the case during the recovery phase of a substorm (when $\vec{E} \times \vec{B}$ convection decreases while the inertia of the massive neutral atmosphere supports the neutral winds for a longer time), this is no longer true, as neutral winds can be a source of electromagnetic energy, in which case they contribute positively to Joule heating. In this case, an estimation of Joule heating without taking into account the presence of neutral winds will lead to its under-estimation. Thus the resulting estimates based on EISCAT can lead to an over-estimation of Joule heating when

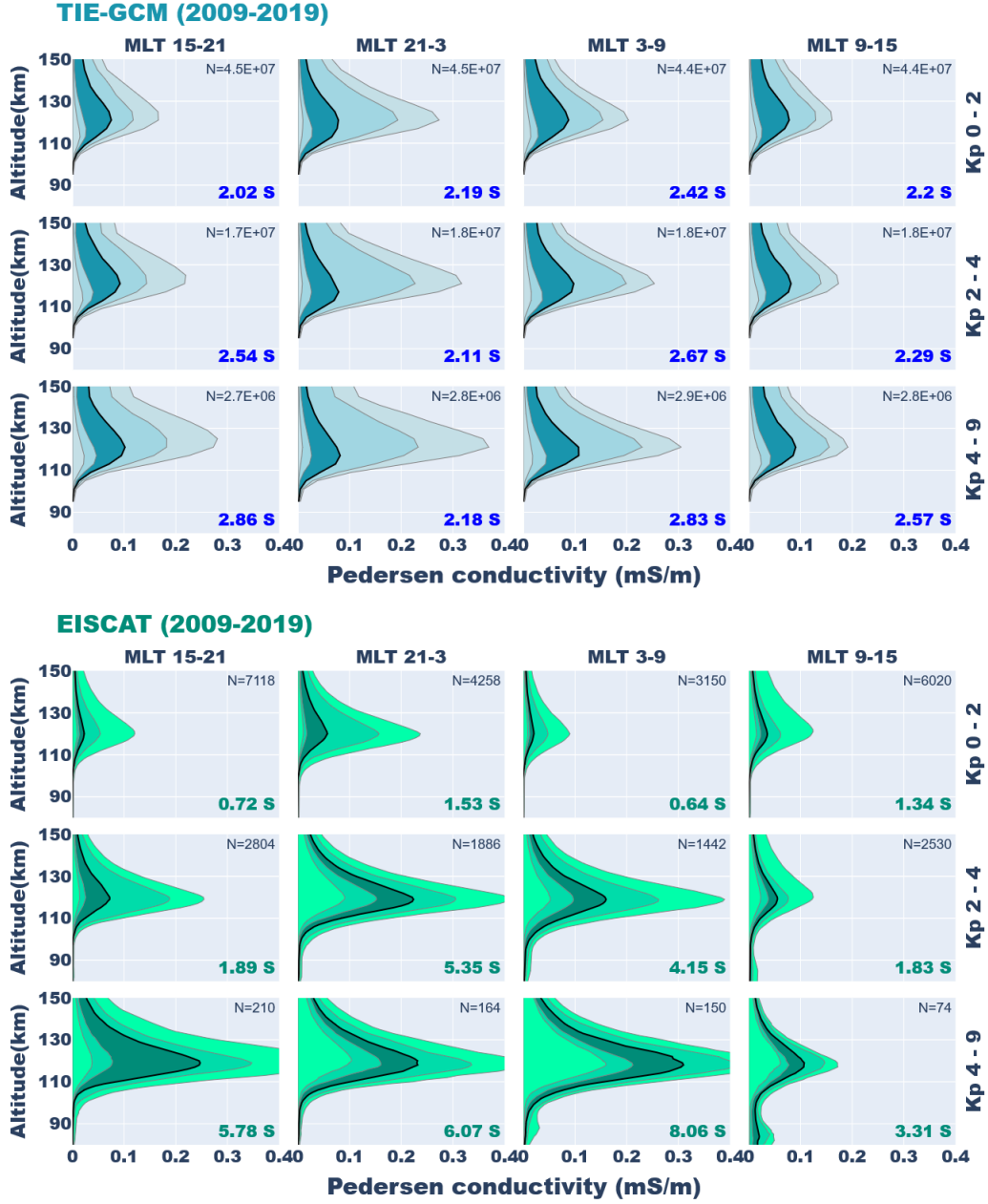


Figure 2. Altitude profiles of Pedersen Conductivity in TIE-GCM (top panel) and EISCAT (bottom panel), in units of mS/m. Marked in blue (green) bold numbers are the height integrated values of the median of Pedersen conductivity in TIE-GCM (EISCAT), in units of *Siemens*; marked in smaller black characters are the number *N* of grid points (top) and samples (bottom) that were used to produce the altitude profiles.

the neutral wind is a sink, or an under-estimation, when the neutral wind is a source of energy.

In order to assess the extent to which the discrepancies between Joule heating in TIE-GCM and EISCAT depend on the effect of the neutral winds on a long-term average, we estimated the Joule heating in TIE-GCM after subtracting the effect of neutral winds. This was done according to equation (12) of T. E. Sarris et al. (2023), where, by expanding equation 1 for Joule heating, we obtain:

$$q_{\Omega} = \sigma_P \left(\vec{E} + \vec{u}_n \times \vec{B} \right)^2 = \underbrace{\sigma_P E^2}_{q_c} + \underbrace{\sigma_P |\vec{u}_n \times \vec{B}|^2 - 2\sigma_P \vec{u}_n \cdot (\vec{E} \times \vec{B})}_{q_w} \quad (4)$$

In the above equation, the term marked as q_c is commonly referred to as convection heating (e.g., Lu et al. (1995b); Billett et al. (2018)), and corresponds to the Joule heating rate in the absence of neutral winds, whereas the second term, marked as q_w , allows for the quantification of the contribution of the neutral winds to Joule heating.

In order to better assess the Kp levels and the areas in local time and altitude where the effects of neutral winds are more evident, in Figure 3 we plot with a solid blue line the median altitude profiles of Joule heating from TIE-GCM with the effects of the neutral winds ($q_c + q_w$) and with a dashed blue line Joule heating in TIE-GCM without including the effect of the neutral winds (q_c only). In this plot, the visual comparison between the median altitude profiles is further quantified arithmetically with the calculation of the percentage difference between the two height-integrated Joule heating estimates that correspond to the areas under the solid and dashed blue lines, respectively. The percentage difference is defined here as the height-integrated value of Joule heating with the effects of neutral winds minus Joule heating without the effects of neutral winds, divided by Joule heating with the effects of neutral winds.

From Figure 3 it can be seen that Joule heating in TIE-GCM without taking into account the effect of the neutral winds is, in most cases, higher than Joule heating when including the effect of neutral winds, except for the morning and noon sections for low Kp values, where Joule heating has the lowest values among all MLT and Kp bins. The effects of the neutral winds maximize in the afternoon sector (MLT 15-21) for all Kp levels, with an average percentage difference of 26.3% in these sectors; whereas the percentage difference when taking into account all local time sectors and all Kp ranges is on average 16.2%.

In comparison, Thayer (1998) used the Sondrestrom ISR to sample currents, conductivities, electric fields, and neutral winds in the E region, and evaluated height-integrated E region Joule heating rates, investigating in particular the influence of the neutral wind on these estimates. They found that the E region height-integrated Joule heating rate for the particular time period they investigated (which corresponded to solar minimum, daytime conditions with periods of moderate to strong geomagnetic activity) experienced an overall decrease of 40% due to the neutral wind. This is higher than the percentage difference found above, but within order of magnitude.

Furthermore, Thayer (1998) found that, whereas neutral winds reduce the local Joule heating rate in the upper E region, they enhance the local Joule heating rate in the lower E region. Looking in closer detail at the altitude profiles in Figure 3, we can see that a similar behaviour is observed in the altitude profiles as obtained from TIE-GCM: for example, the dashed line (no neutral wind) in the MLT 15-21 sector for the Kp 4-9 range exceeds the values of the solid line (with neutral wind) at altitudes above 120 km, but has lower values than the solid line at altitudes below 120 km.

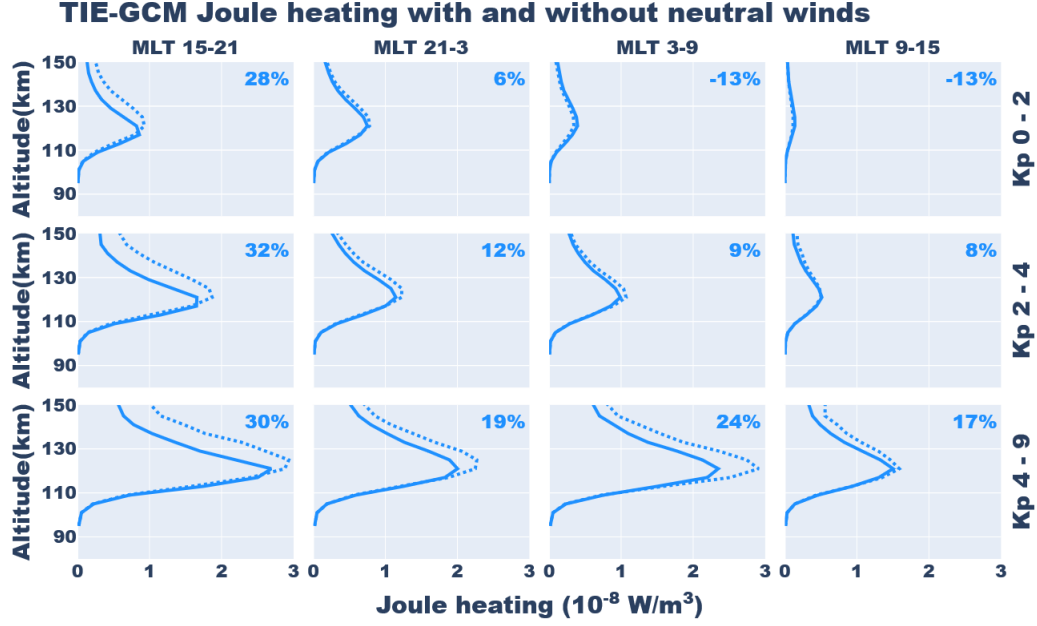


Figure 3. Comparison of Joule heating as calculated in TIE-GCM with (solid line) and without (dashed line) the effects of the neutral winds. The number at each sub-figure marks the percentage difference between the height-integrated value of Joule heating with the effects of neutral winds and without the effects of neutral winds, divided by Joule heating with the effects of neutral winds

From the above estimates and the calculated percentage differences, it is noted that the effect of the neutral winds cannot account for the differences between TIE-GCM and EISCAT, shown in the purple percentages that are listed in the lower right corner of each panel.

Another source of uncertainty in the calculations of Joule heating involves the spatio-temporal resolution of the estimation methodology. It is well known that small scale variations can contribute significantly to the total Joule heating (e.g., Emery et al. (1999); Matsuo et al. (2001); Matsuo and Richmond (2008); Q. Zhu et al. (2018)). This is primarily due to the fact that variations of the electric field around a mean do not average to zero, as the square of the electric field contributes to Joule heating in equation 1. For example, electric fields below 10 km are known to be significant at times, with variability at these scales often exceeding the average. Joule heating in TIE-GCM is calculated in a grid of 2.5° in both latitude and longitude, corresponding to a spatial resolution on the order of ~ 280 km in the meridional direction and ~ 80 km in the azimuthal direction at auroral latitudes; it is thus expected that TIE-GCM cannot resolve small-scale variability. In comparison, the EISCAT beam-swing method utilized in this study for electric field estimates results in horizontal spatial resolutions on the order of several tens of km. In order for TIE-GCM to obtain neutral temperatures that are in agreement with statistical observations, such as are obtained, for example, via NRLMSISE-00 (Picone et al. (2002)), TIE-GCM in the estimate of Joule heating includes an empirically-derived multiplication factor, termed JOULEFAC, which increases Joule heating by a fixed factor of 1.5 by default, to account for sub-grid-scale and related effects (see, e.g., NCAR (2016)). As noted in, e.g., Release 1.9 of TIE-GCM, the value of JOULEFAC is a matter of debate, and its value has been replaced/adjusted in several studies to other fixed levels; for example, Emery et al. (1999) needed to multiply the calculated Joule heat-

ing by 2.5 in the northern hemisphere and by 1.5 in the southern hemisphere during the 2 – 11 November 1993 storm event in order to reproduce observed thermospheric responses. The results from the comparison presented above indicate that a Kp-dependent, variable Joule heating factor, $\text{JouleFAC}(\text{Kp})$ that results in lower Joule heating for lower levels of geomagnetic activity and higher Joule heating for higher levels of geomagnetic activity would lead to a closer agreement between TIE-GCM and EISCAT.

Finally, it is noted that the temporal scales over which Joule heating is resolved in TIE-GCM and EISCAT could also contribute to inaccuracies in Joule heating and Pedersen conductivity and resulting discrepancies between the two estimation methodologies. For example, as discussed in Rodger et al. (2001), a low time resolution in EISCAT will generally lead to an underestimation of Joule heating. In this study, the time resolution for Pedersen conductivity is ~ 1 min and for the electric field it is ~ 6 min, leading to a time resolution for Joule heating of ~ 1 min. This is within the range of temporal resolutions used in past studies; e.g., Aikio and Selkälä (2009) used a resolution of ~ 2 min for both the electric field and conductivity in the tri-static EISCAT data analysis. The effect of different time resolutions in TIE-GCM and EISCAT on the resulting Joule heating needs to be further explored through parametric studies, and is beyond the scope of this study.

5 Summary and Conclusions

In this work, Joule heating rates and Pedersen conductivity were calculated statistically as a function of altitude, magnetic local time (MLT) and geomagnetic activity (Kp), using a long-term (11 year) simulation of the lower thermosphere-ionosphere based on TIE-GCM and a corresponding period of EISCAT radar observations. Model and radar data were obtained from 2009 until 2019 for both methodologies. Through this comparison, it was found that both the TIE-GCM run and EISCAT estimates agree on the shape of the altitude distribution. With respect to the approximate altitude of the peak in Joule Heating and Pedersen Conductivity distributions, the maximum value of Joule heating and Pedersen conductivity are found at ~ 120 km of altitude in both TIE-GCM run and EISCAT.

By subtracting the effect of neutral winds from the estimates of Joule heating in TIE-GCM, it is found that neutral winds can account, on average, for $\sim 16.2\%$ of Joule heating in TIE-GCM. An MLT dependence is found in the effect of the neutral winds, with strongest effects appearing in the afternoon ($\sim 26.3\%$), followed by the other sectors ($\sim 12\%$).

It is concluded that this difference cannot account for the discrepancies in Joule heating between TIE-GCM and EISCAT, and thus, that the largest effect leading to the discrepancies between the Joule heating estimations in TIE-GCM and EISCAT are not due to the lack of neutral wind velocities when estimating Joule heating in EISCAT. Instead, these discrepancies should probably be attributed to small-scale effects that amount to sub-grid variability that cannot be resolved in TIE-GCM, and which are currently parameterized/adjusted by a multiplication factor, or to the lack of small temporal scales in TIE-GCM. It was also found that TIE-GCM tends to under-estimate both Joule heating and Pedersen conductivity for high levels of geomagnetic activity and, inversely, to over-estimate their values for low levels of geomagnetic activity, compared to EISCAT measurements. This suggests that replacing the constant multiplication factor, JouleFAC , that is currently used in TIE-GCM by a Kp-dependent factor would yield better results for both low and high activity levels.

The results presented herein underline the need for more accurate knowledge of the contribution of all relevant spatial and temporal scales, which is paramount to accurately parameterize Joule heating in models such as TIE-GCM. Revealing and accurately re-

solving the contribution of all scales of interest to Joule heating, while including the contributions of all parameters involved, is best achieved by in situ measurements of the lower thermosphere - ionosphere, as it has been emphasized in many recent studies (e.g., Heelis and Maute (2020); T. E. Sarris et al. (2020); Palmroth et al. (2021); T. Sarris et al. (2023)). Further to the improvements in the unambiguous characterization of Joule heating that will be enabled through comprehensive in situ observations in the LTI, improvement of models will also emerge from the upcoming developments in radars: for example, the enhanced spatial and temporal resolution that will be offered by EISCAT_3D, currently under development, will greatly improve estimates of Joule heating in small scales (Stamm et al. (2021)). In addition, the planned scanning Fabry-Perot Interferometer (FPI) facility that will be implemented around EISCAT_3D will be a key step in incorporating the effects of neutral winds in the resulting Joule heating. The combination of EISCAT_3D measurements with in situ measurements from a spacecraft mission quantifying the variability of the electric fields and all involved parameters in small scales, such as described in, e.g., T. Sarris et al. (2023), will enable resolving conclusively the key missing pieces of Joule heating and Pedersen conductivity in the LTI.

6 Open Research

Data availability: The EISCAT data are available in the Madrigal database: <https://madrigal.eiscat.se/madrigal/>

TIE-GCM source code: The NCAR Thermosphere-Ionosphere-Electrodynamics General Circulation Model (TIE-GCM) can be downloaded from <https://www.hao.ucar.edu/modeling/tgcm/tie.php>

Data processing source code: The processing of TIE-GCM output data and EISCAT data was done using the code that can be found at: https://github.com/baldimitris/TIEGCM_Statistics (Baloukidis et al. (2023)).

Acknowledgments

We thank the EISCAT Scientific Association for providing the incoherent scatter radar data used in this study. EISCAT is an international association supported by research organisations in China (CRIRP), Finland (SA), Japan (NIPR and ISEE), Norway (NFR), Sweden (VR), and the United Kingdom (UKRI). The EISCAT data are available in the Madrigal database: <https://madrigal.eiscat.se/madrigal/>.

This work was supported by the Kvantum Institute of the University of Oulu and by the Academy of Finland (347796 and 24304299).

References

- Aikio, A. T., Cai, L., & Nygrén, T. (2012). Statistical distribution of height-integrated energy exchange rates in the ionosphere. *Journal of Geophysical Research: Space Physics*, 117(A10). Retrieved from <https://agupubs.onlinelibrary.wiley.com/doi/abs/10.1029/2012JA018078> doi: <https://doi.org/10.1029/2012JA018078>
- Aikio, A. T., & Selkälä, A. (2009). Statistical properties of joule heating rate, electric field and conductances at high latitudes. *Annales Geophysicae*, 27(7), 2661–2673. Retrieved from <https://angeo.copernicus.org/articles/27/2661/2009/> doi: 10.5194/angeo-27-2661-2009
- Baloukidis, D., Tourgaidis, S., Pirnaris, P., & Papadakis, K. (2023). *Software for statistical analysis of tie-gcm calculated joule heating and pedersen conductivity and comparison with eiscat data*. [Source code]. Zenodo. Re-

- trieved from <https://github.com/baldimitris/TIEGCM.Statistics> doi:
<https://zenodo.org/badge/latestdoi/618768694>
- Banks, P. (1977). Observations of joule and particle heating in the auroral zone. *Journal of Atmospheric and Terrestrial Physics*, 39(2), 179-193. Retrieved from <https://www.sciencedirect.com/science/article/pii/002191697790112X> doi: [https://doi.org/10.1016/0021-9169\(77\)90112-X](https://doi.org/10.1016/0021-9169(77)90112-X)
- Billett, D., Grocott, A., Wild, J., Walach, M.-T., & Kosch, M. (2018). Diurnal variations in global joule heating morphology and magnitude due to neutral winds. *Journal of Geophysical Research: Space Physics*, 123(3), 2398-2411.
- Brekke, A., & Hall, C. (1988, August). Auroral ionospheric quiet summer time conductances. *Annales Geophysicae*, 6, 361-375.
- Brekke, A., & Kamide, Y. (1996). On the relationship between joule and frictional heating in the polar ionosphere. *Journal of Atmospheric and Terrestrial Physics*, 58(1), 139-143. Retrieved from <https://www.sciencedirect.com/science/article/pii/0021916995000259> (Selected papers from the sixth international Eiscat Workshop) doi: [https://doi.org/10.1016/0021-9169\(95\)00025-9](https://doi.org/10.1016/0021-9169(95)00025-9)
- Brekke, A., & Rino, C. L. (1978). High-resolution altitude profiles of the auroral zone energy dissipation due to ionospheric currents. *Journal of Geophysical Research: Space Physics*, 83(A6), 2517-2524. Retrieved from <https://agupubs.onlinelibrary.wiley.com/doi/abs/10.1029/JA083iA06p02517> doi: <https://doi.org/10.1029/JA083iA06p02517>
- Cai, L., Aikio, A. T., & Nygrén, T. (2013). Height-dependent energy exchange rates in the high-latitude e region ionosphere. *Journal of Geophysical Research: Space Physics*, 118(11), 7369-7383. Retrieved from <https://agupubs.onlinelibrary.wiley.com/doi/abs/10.1002/2013JA019195> doi: <https://doi.org/10.1002/2013JA019195>
- Cole, K. D. (1962). Joule heating of the upper atmosphere. *Australian Journal of Physics*, 15(2), 223-235. Retrieved from <https://doi.org/10.1071/PH620223> doi: 10.1071/PH620223
- Deng, Y., & Ridley, A. J. (2007). Possible reasons for underestimating joule heating in global models: E field variability, spatial resolution, and vertical velocity. *Journal of Geophysical Research: Space Physics*, 112(A9). Retrieved from <https://agupubs.onlinelibrary.wiley.com/doi/abs/10.1029/2006JA012006> doi: <https://doi.org/10.1029/2006JA012006>
- Emery, B., Lathuillere, C., Richards, P., Roble, R., Buonsanto, M., Knipp, D., ... Niciejewski, R. (1999). Time dependent thermospheric neutral response to the 2-11 november 1993 storm period. *Journal of Atmospheric and Solar-Terrestrial Physics*, 61(3), 329-350. Retrieved from <https://www.sciencedirect.com/science/article/pii/S1364682698001370> doi: [https://doi.org/10.1016/S1364-6826\(98\)00137-0](https://doi.org/10.1016/S1364-6826(98)00137-0)
- Emery, B., Roble, R. G., Ridley, E. C., Richmond, A. D., Knipp, D. J., Crowley, G., ... Maeda, S. (2012). Parameterization of the ion convection and the auroral oval in the near thermospheric general circulation models. *NCAR Tech. Note NCAR/TN-491+ STR*. doi: 10.5065/D6N29TXZ
- Fujii, R., Nozawa, S., Buchert, S. C., & Brekke, A. (1999). Statistical characteristics of electromagnetic energy transfer between the magnetosphere, the ionosphere, and the thermosphere. *Journal of Geophysical Research: Space Physics*, 104(A2), 2357-2365. Retrieved from <https://agupubs.onlinelibrary.wiley.com/doi/abs/10.1029/98JA02750> doi: <https://doi.org/10.1029/98JA02750>
- Griffis, M., Nisbet, J., & Bleuler, E. (1981). Particle and joule heating of the neutral polar thermosphere in cusp region using atmosphere explorer-c satellite measurements. *Advances in Space Research*, 1(12), 27-30. Retrieved from <https://www.sciencedirect.com/science/article/pii/0273117781904130> doi: [https://doi.org/10.1016/0273-1177\(81\)90413-0](https://doi.org/10.1016/0273-1177(81)90413-0)

- Heelis, R. A., & Maute, A. (2020, February). Challenges to Understanding the Earth's Ionosphere and Thermosphere. *Journal of Geophysical Research: Space Physics*, 125(7). doi: 10.1029/2019JA027497
- Huang, Y., Richmond, A. D., Deng, Y., & Roble, R. (2012). Height distribution of joule heating and its influence on the thermosphere. *Journal of Geophysical Research: Space Physics*, 117(A8). Retrieved from <https://agupubs.onlinelibrary.wiley.com/doi/abs/10.1029/2012JA017885> doi: <https://doi.org/10.1029/2012JA017885>
- Knipp, D., Welliver, T., McHarg, M., Chun, F., Tobiska, W., & Evans, D. (2005). Climatology of extreme upper atmospheric heating events. *Advances in Space Research*, 36(12), 2506-2510. Retrieved from <https://www.sciencedirect.com/science/article/pii/S0273117705002103> (Space Weather) doi: <https://doi.org/10.1016/j.asr.2004.02.019>
- Lu, G., Richmond, A., Emery, B., & Roble, R. (1995b). Magnetosphere-ionosphere-thermosphere coupling: Effect of neutral winds on energy transfer and field-aligned current. *Journal of Geophysical Research: Space Physics*, 100(A10), 19643-19659.
- Lu, G., Richmond, A. D., Emery, B. A., & Roble, R. G. (1995a). Magnetosphere-ionosphere-thermosphere coupling: Effect of neutral winds on energy transfer and field-aligned current. *Journal of Geophysical Research: Space Physics*, 100(A10), 19643-19659. Retrieved from <https://agupubs.onlinelibrary.wiley.com/doi/abs/10.1029/95JA00766> doi: <https://doi.org/10.1029/95JA00766>
- Lu, G., Richmond, A. D., Lühr, H., & Paxton, L. (2016). High-latitude energy input and its impact on the thermosphere. *Journal of Geophysical Research: Space Physics*, 121(7), 7108-7124. Retrieved from <https://agupubs.onlinelibrary.wiley.com/doi/abs/10.1002/2015JA022294> doi: <https://doi.org/10.1002/2015JA022294>
- Matsuo, T., & Richmond, A. D. (2008). Effects of high-latitude ionospheric electric field variability on global thermospheric joule heating and mechanical energy transfer rate. *Journal of Geophysical Research: Space Physics*, 113(A7). Retrieved from <https://agupubs.onlinelibrary.wiley.com/doi/abs/10.1029/2007JA012993> doi: <https://doi.org/10.1029/2007JA012993>
- Matsuo, T., Richmond, A. D., & Nychka, D. W. (2001, December). Modes of the High-Latitude Electric Field Variability Derived From DE-2 Measurements: Empirical Orthogonal Function (EOF) Analysis. In *Agu fall meeting abstracts* (Vol. 2001, p. SA32A-0689).
- Moen, J., Brekke, A., & Hall, C. (1990). An attempt to derive electron energy spectra for auroral daytime precipitation events. *Journal of Atmospheric and Terrestrial Physics*, 52(6), 459-471. Retrieved from <https://www.sciencedirect.com/science/article/pii/0021916990900450> (The Fourth International EISCAT Workshop) doi: [https://doi.org/10.1016/0021-9169\(90\)90045-O](https://doi.org/10.1016/0021-9169(90)90045-O)
- NCAR, H. A. O. (2016). *Tiegcmm documentation, release 2.0*. Retrieved 2016-03-21, from <https://www.hao.ucar.edu/modeling/tgcm/tiegcmm2.0/userguide/userguide.pdf> (Accessed: 27-3-2023)
- Nygrén, T., Aikio, T., A., Kuula, R., & Voiculescu, M. (2011). Electric fields and neutral winds from monostatic incoherent scatter measurements by means of stochastic inversion. *Journal of Geophysical Research: Space Physics*, 116(A5). Retrieved from <https://agupubs.onlinelibrary.wiley.com/doi/abs/10.1029/2010JA016347> doi: <https://doi.org/10.1029/2010JA016347>
- Palmroth, M., Grandin, M., Sarris, T., Doornbos, E., Tourgaidis, S., Aikio, A., ... Yamauchi, M. (2020, 07). Lower thermosphere – ionosphere (lti) quantities: Current status of measuring techniques and models. *Annales Geophysicae Discussions*. doi: 10.5194/angeo-2020-42
- Palmroth, M., Grandin, M., Sarris, T., Doornbos, E., Tourgaidis, S., Aikio, A., ...

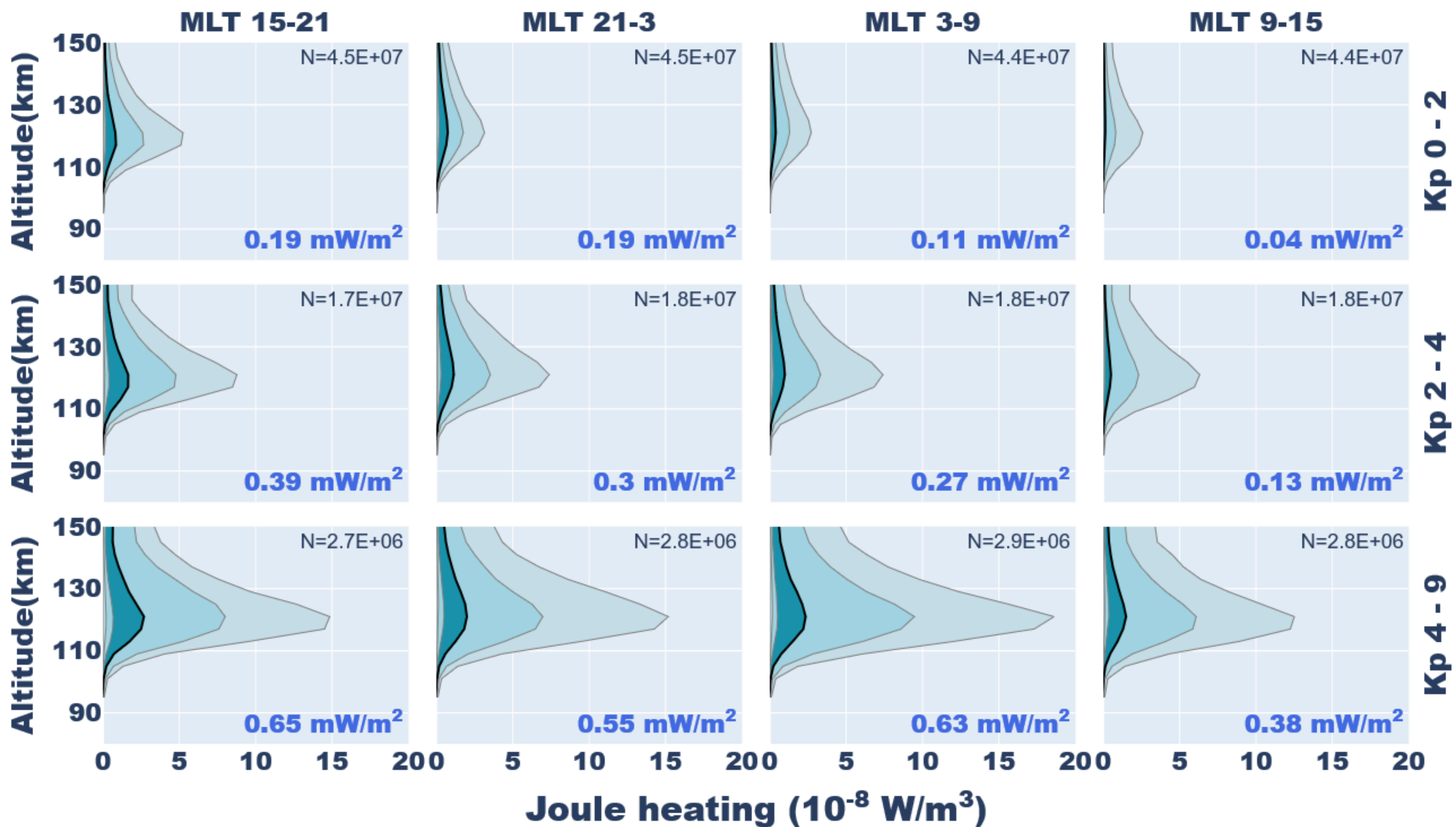
- others (2021). Lower-thermosphere–ionosphere (lti) quantities: current status of measuring techniques and models. In *Annales geophysicae* (Vol. 39, pp. 189–237).
- Palmroth, M., Janhunen, P., Pulkkinen, T. I., Aksnes, A., Lu, G., Østgaard, N., ... Germany, G. A. (2005). Assessment of ionospheric joule heating by gumics-4 mhd simulation, amie, and satellite-based statistics: towards a synthesis. *Annales Geophysicae*, 23(6), 2051–2068. Retrieved from <https://angeo.copernicus.org/articles/23/2051/2005/> doi: 10.5194/angeo-23-2051-2005
- Perlongo, N. J., Ridley, A. J., Cnossen, I., & Wu, C. (2018, February). A Year-Long Comparison of GPS TEC and Global Ionosphere-Thermosphere Models. *JGR Space Physics*, 123(2), 1410–1428. doi: 10.1002/2017JA024411
- Picone, J. M., Hedin, A. E., Drob, D. P., & Aikin, A. C. (2002). Nrlmsise-00 empirical model of the atmosphere: Statistical comparisons and scientific issues. *Journal of Geophysical Research: Space Physics*, 107(A12), SIA 15-1–SIA 15-16. Retrieved from <https://agupubs.onlinelibrary.wiley.com/doi/abs/10.1029/2002JA009430> doi: <https://doi.org/10.1029/2002JA009430>
- Qian, L., Burns, A. G., Emery, B. A., Foster, B., Lu, G., Maute, A., ... Wang, W. (2014). The near tie-gcm. In *Modeling the ionosphere–thermosphere system* (p. 73–83). American Geophysical Union (AGU). Retrieved from <https://agupubs.onlinelibrary.wiley.com/doi/abs/10.1002/9781118704417.ch7> doi: <https://doi.org/10.1002/9781118704417.ch7>
- Roble, R. G., & Ridley, E. C. (1987, December). An auroral model for the NCAR thermospheric general circulation model (TGCM). *Annales Geophysicae*, 5, 369–382.
- Rodger, A. S., Wells, G. D., Moffett, R. J., & Bailey, G. J. (2001). The variability of joule heating, and its effects on the ionosphere and thermosphere. *Annales Geophysicae*, 19(7), 773–781. Retrieved from <https://angeo.copernicus.org/articles/19/773/2001/> doi: 10.5194/angeo-19-773-2001
- Ruan, H., Lei, J., Dou, X., Liu, S., & Aa, E. (2018, February). An Exospheric Temperature Model Based On CHAMP Observations and TIEGCM Simulations. *AGU Space Weather*, 16(2). doi: 10.1002/2017SW001759
- Sangalli, L., Knudsen, J., D., Larsen, F., M., Zhan, T., Pfaff, F., R., & Rowland, D. (2009, April). Rocket-based measurements of ion velocity, neutral wind, and electric field in the collisional transition region of the auroral ionosphere. *AGU Journal of Geophysical Research*, 114(A4). doi: 10.1029/2008JA013757
- Sarris, T., Palmroth, M., Aikio, A., Buchert, S. C., Clemmons, J., Clilverd, M., ... Yamauchi, M. (2023). Plasma-neutral interactions in the lower thermosphere-ionosphere: The need for in situ measurements to address focused questions. *Frontiers in Astronomy and Space Sciences*, 9. Retrieved from <https://www.frontiersin.org/articles/10.3389/fspas.2022.1063190> doi: 10.3389/fspas.2022.1063190
- Sarris, T. E. (2019, May). Understanding the ionosphere thermosphere response to solar and magnetospheric drivers: status, challenges and open issues. *Phil. Trans. R. Soc. A*, 377(2148). doi: 10.1098/rsta.2018.0101
- Sarris, T. E., Talaat, E. R., Palmroth, M., Dandouras, I., Armandillo, E., Kervalishvili, G., ... Aikio, A. (2020). Daedalus: a low-flying spacecraft for in situ exploration of the lower thermosphere–ionosphere. *Geoscientific Instrumentation, Methods and Data Systems*, 9(1), 153–191. Retrieved from <https://gi.copernicus.org/articles/9/153/2020/> doi: 10.5194/gi-9-153-2020
- Sarris, T. E., Tourgaidis, S., Pirnaris, P., Baloukidis, D., Papadakis, K., Psychalas, C., ... Stachlys, N. (2023). Daedalus mase (mission assessment through simulation exercise): A toolset for analysis of in situ missions and for processing global circulation model outputs in the lower thermosphere-

- ionosphere. *Frontiers in Astronomy and Space Sciences*, 9. Retrieved from <https://www.frontiersin.org/articles/10.3389/fspas.2022.1048318> doi: 10.3389/fspas.2022.1048318
- Scherliess, L., Tsagouri, I., Yizengaw, E., Bruinsma, S., Shim, J. S., Coster, A., & Retterer, J. M. (2019). The international community coordinated modeling center space weather modeling capabilities assessment: Overview of ionosphere/thermosphere activities. *Space Weather*, 17(4), 527-538. Retrieved from <https://agupubs.onlinelibrary.wiley.com/doi/abs/10.1029/2018SW002036> doi: <https://doi.org/10.1029/2018SW002036>
- Chunk, R. W., & Nagy, A. F. (2000). *Ionospheres: Physics, plasma physics, and chemistry*. Cambridge University Press. doi: 10.1017/CBO9780511551772
- Stamm, J., Vierinen, J., & Gustavsson, B. (2021). Observing electric field and neutral wind with eiscat 3d. *Annales Geophysicae*, 39(6), 961-974. Retrieved from <https://angeo.copernicus.org/articles/39/961/2021/> doi: 10.5194/angeo-39-961-2021
- Strangeway, R. J. (2012). The equivalence of joule dissipation and frictional heating in the collisional ionosphere. *Journal of Geophysical Research: Space Physics*, 117(A2). Retrieved from <https://agupubs.onlinelibrary.wiley.com/doi/abs/10.1029/2011JA017302> doi: <https://doi.org/10.1029/2011JA017302>
- Thayer, J. P. (1998). Height-resolved joule heating rates in the high-latitude E region and the influence of neutral winds. *Journal of Geophysical Research: Space Physics*, 103(A1), 471-487. Retrieved from <https://agupubs.onlinelibrary.wiley.com/doi/abs/10.1029/97JA02536> doi: <https://doi.org/10.1029/97JA02536>
- Thayer, J. P. (2000). High-latitude currents and their energy exchange with the ionosphere-thermosphere system. *Journal of Geophysical Research: Space Physics*, 105(A10), 23015-23024. Retrieved from <https://agupubs.onlinelibrary.wiley.com/doi/abs/10.1029/1999JA000409> doi: <https://doi.org/10.1029/1999JA000409>
- Thayer, J. P., & Semeter, J. (2004). The convergence of magnetospheric energy flux in the polar atmosphere. *Journal of Atmospheric and Solar-Terrestrial Physics*, 66(10), 807-824. Retrieved from <https://www.sciencedirect.com/science/article/pii/S1364682604000537> (Upper Atmosphere Tutorials from the 2001 Joint CEDAR SCOSTEP Meeting) doi: <https://doi.org/10.1016/j.jastp.2004.01.035>
- Thébault, E., Finlay, C. C., Beggan, C. D., Alken, P., Aubert, J., Barrois, O., ... others (2015). International geomagnetic reference field: the 12th generation. *Earth, Planets and Space*, 67(1), 1-19.
- Vasyliūnas, V. M., & Song, P. (2005). Meaning of ionospheric joule heating. *Journal of Geophysical Research: Space Physics*, 110(A2). Retrieved from <https://agupubs.onlinelibrary.wiley.com/doi/abs/10.1029/2004JA010615> doi: <https://doi.org/10.1029/2004JA010615>
- Vickrey, J. F., Vondrak, R. R., & Matthews, S. J. (1982). Energy deposition by precipitating particles and joule dissipation in the auroral ionosphere. *Journal of Geophysical Research: Space Physics*, 87(A7), 5184-5196. Retrieved from <https://agupubs.onlinelibrary.wiley.com/doi/abs/10.1029/JA087iA07p05184> doi: <https://doi.org/10.1029/JA087iA07p05184>
- Weimer, D. R. (2005). Improved ionospheric electrodynamic models and application to calculating joule heating rates. *Journal of Geophysical Research: Space Physics*, 110(A5). Retrieved from <https://agupubs.onlinelibrary.wiley.com/doi/abs/10.1029/2004JA010884> doi: <https://doi.org/10.1029/2004JA010884>
- Wickwar, V. B. (1974, January). *Analysis techniques for incoherent-scatter data interpretation in the 100-300 km region*.
- Zhu, Q., Deng, Y., Richmond, A., & Maute, A. (2018). Small-scale and mesoscale

variabilities in the electric field and particle precipitation and their impacts on
 joule heating. *Journal of Geophysical Research: Space Physics*, 123(11), 9862-
 9872. Retrieved from [https://agupubs.onlinelibrary.wiley.com/doi/abs/](https://agupubs.onlinelibrary.wiley.com/doi/abs/10.1029/2018JA025771)
 10.1029/2018JA025771 doi: <https://doi.org/10.1029/2018JA025771>
 Zhu, X., Talaat, E. R., Baker, J. B. H., & Yee, J.-H. (2005). A self-consistent
 derivation of ion drag and joule heating for atmospheric dynamics in the
 thermosphere. *Annales Geophysicae*, 23(10), 3313–3322. Retrieved
 from <https://angeo.copernicus.org/articles/23/3313/2005/> doi:
 10.5194/angeo-23-3313-2005

Figure 1.

TIE-GCM (2009-2019)



EISCAT (2009-2019)

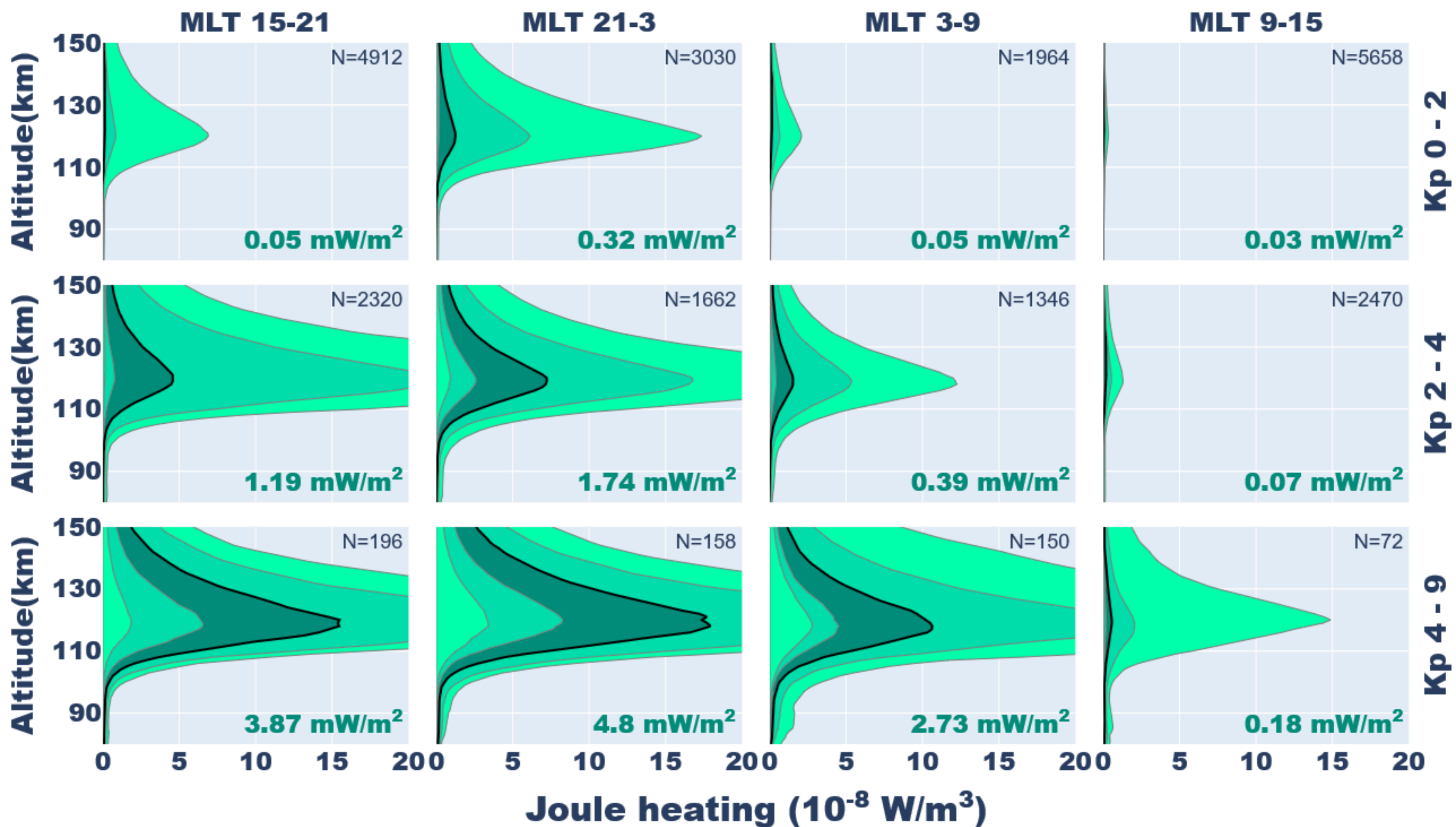
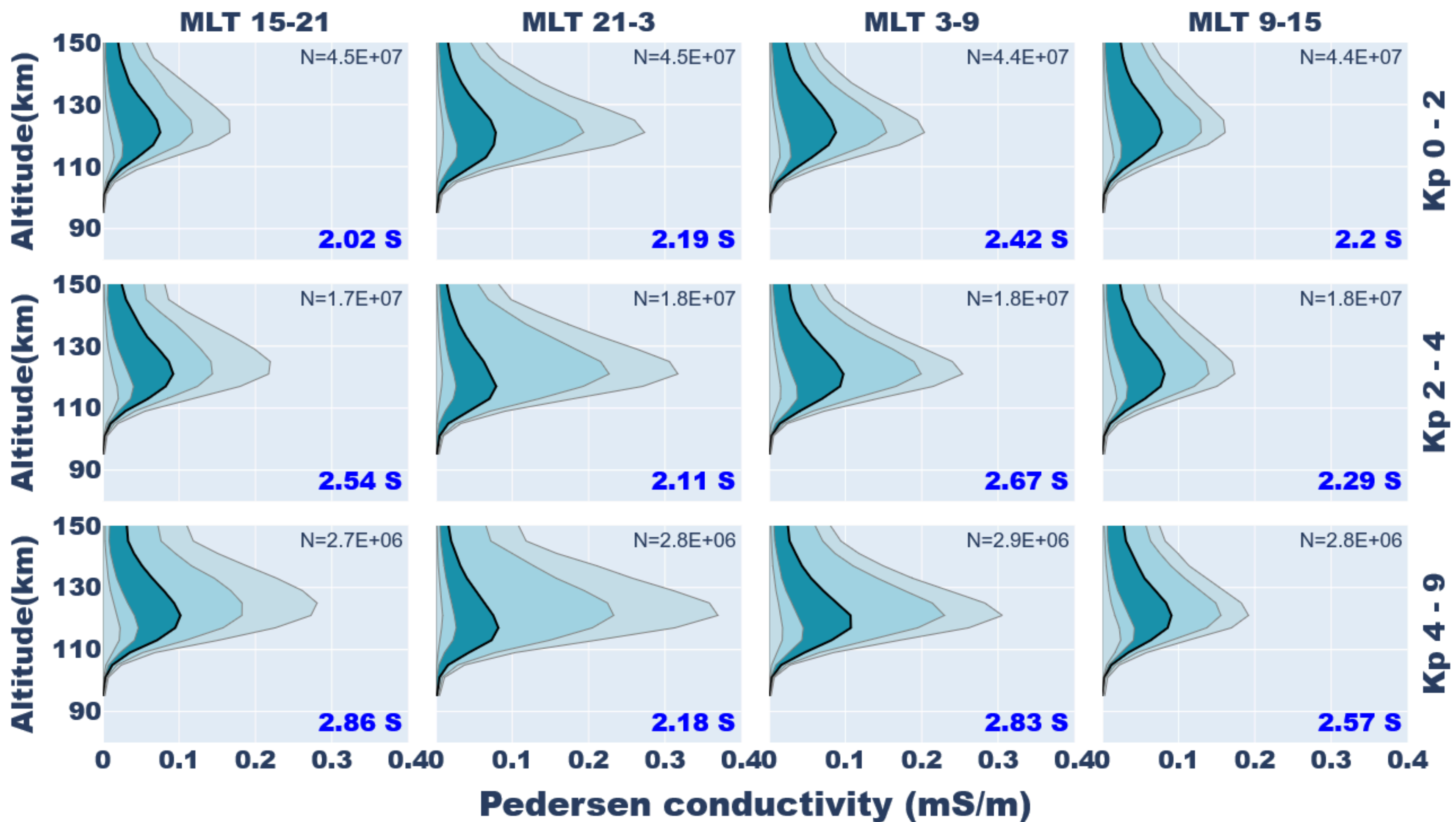


Figure 2.

TIE-GCM (2009-2019)



EISCAT (2009-2019)

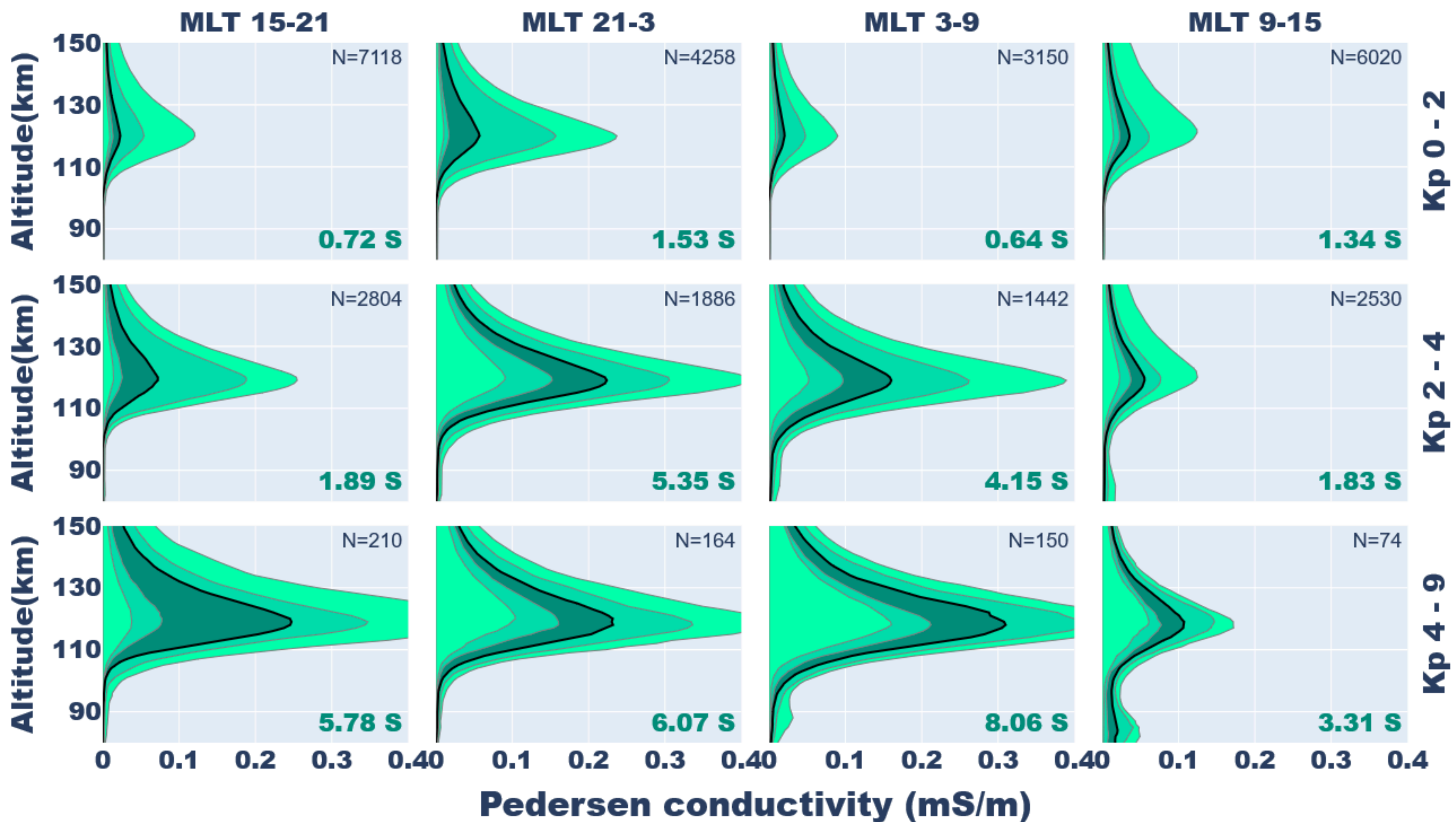


Figure 3.

TIE-GCM Joule heating with and without neutral winds

